Article

Easily Processable Phenylene–Thiophene-Based Organic Field-Effect Transistors and Solution-Fabricated Nonvolatile Transistor Memory Elements

Melissa Mushrush, Antonio Facchetti, Michael Lefenfeld, Howard E. Katz, and Tobin J. Marks

J. Am. Chem. Soc., **2003**, 125 (31), 9414-9423• DOI: 10.1021/ja035143a • Publication Date (Web): 15 July 2003

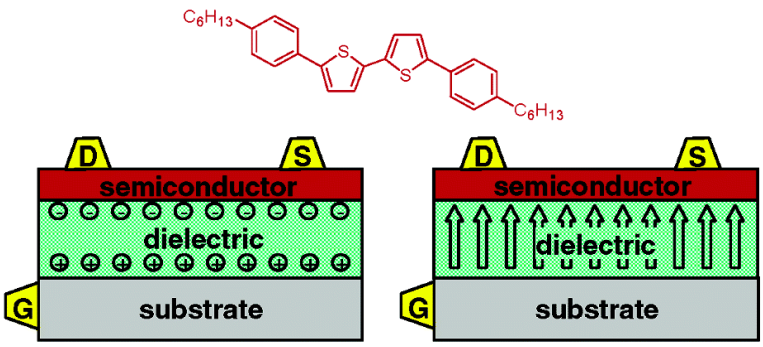

More About This Article

Additional resources and features associated with this article are available within the HTML version:

- Supporting Information
- Links to the 47 articles that cite this article, as of the time of this article download
- Access to high resolution figures
- Links to articles and content related to this article
- Copyright permission to reproduce figures and/or text from this article

View the Full Text HTML

J|A|C|S
ARTICLES
Published on Web 07/15/2003

Easily Processable Phenylene−Thiophene-Based Organic Field-Effect Transistors and Solution-Fabricated Nonvolatile Transistor Memory Elements

Melissa Mushrush,[†] Antonio Facchetti,[†] Michael Lefenfeld,[‡] Howard E. Katz,*[,‡] and Tobin J. Marks*[,†]

Contribution from the Department of Chemistry and the Materials Research Center, Northwestern University, 2145 Sheridan Road, Evanston, Illinois 60208-3113 and Bell Laboratories, Lucent Technologies, 600 Mountain Avenue, Murray Hill, New Jersey 07974

Received March 13, 2003; E-mail: hek@lucent.com; t-marks@northwestern.edu

Abstract: The synthesis of a new series of mixed phenylene−thiophene oligomers is reported; 2,5-bis(4-*n*-hexylphenyl)thiophene (dH-PTP, **1**), 5,5′-bis(4-*n*-hexylphenyl)-2,2′-bithiophene (dH-PTTP, **2**), 5,5″-bis-(4-*n*-hexylphenyl)-2,2′:5′,2″-terthiophene (dH-PT_3P, **3**), 5,5‴-bis(4-*n*-hexylphenyl)-2,2′:5′,2″:5″,2‴-quaterthiophene (dH-PT_4P, **4**), 1,4-bis[5-(4-*n*-hexylphenyl)-2-thienyl]benzene (dH-PTPTP, **5**), and 2,5-bis[4(4′-*n*-hexylphenyl)phenyl]thiophene (dH-PPTPP, **6**) were characterized by ^{1}H NMR, elemental analysis, UV−visible spectroscopy, differential scanning calorimetry, and thermogravimetric analysis. Vacuum-evaporated and solution-cast films were characterized by X-ray diffraction and scanning electron microscopy. All compounds display high p-type carrier mobilities as evaporated (up to 0.09 cm^2/Vs) and as solution-cast (up to 0.03 cm^2/Vs) films on both Si/SiO_2 and ITO/GR (glass resin) substrates. The straightforwardly synthesized dH-PTTP (**2**) displays an unprecedented combination of mobility, on/off ratio, stability, and processability. Both dH-PTTP (**2**) and dH-PPTPP (**6**) display a reversible, tunable, and stable memory effect even as solution-cast devices, with turn-on characteristics shifting from accumulation mode to zero or depletion mode after a writing voltage V_w is applied. The charge storage is distributed over the gate dielectric structure and is concentrated near the dielectric−semiconductor interface, as evidenced by the response of "floating gate" configuration devices. Simple nonvolatile elements have been fabricated by solution-only techniques on ITO substrates using spin-coated glass resin, solution-cast oligomeric semiconductors, and painted graphite paste electrodes.

Introduction

Organic semiconductors employed as active layers in field-effect transistors (FETs) are of great current interest because such FETs can potentially be fabricated at low cost, over large areas, and on flexible substrates.[1] Such facile fabrication approaches offer a significant advantage over silicon technology in numerous applications where the performance level of silicon is not essential. Organic semiconductors have now reached impressive levels of performance and depth of understanding.[1,2] Concurrently, substantial progress has been made in various organic-based electronic circuits, such as displays,[3] inverters and logic elements,[4] sensors,[5] and photovoltaic cells.[6] Nevertheless, very few current-generation organic semiconductors simultaneously meet the criteria of high carrier mobility, low leakage current, straightforward synthesis, facile film deposition,[7] and chemical stability. Furthermore, the use of organic transistors as nonvolatile devices that could function as tunable/adaptive elements or information storage buffers, while attractive, has not been extensively pursued.

While the nonvolatile transistor memory element is a well-known device in conventional silicon electronics,[8] it has only

[†] Northwestern University.
[‡] Lucent Technologies.

(1) (a) Pope, M.; Swenberg, C. E. *Electronic Processes in Organic Crystals and Polymers*; Oxford University Press: Oxford, 1999. (b) Dimitrakopoulos, C. D.; Malenfant, P. R. L. *Adv. Mater.* **2002**, *14* (2), 99. (c) Horowitz, G. *J. Mater. Chem.* **1999**, *9*, 2021. (d) Horowitz, G. *Adv. Mater.* **1998**, *10* (5), 365.

(2) (a) Marks, T. J.; Facchetti, A. WO Patent 0,310,778, 2003. (b) Facchetti, A.; Mushrush, M.; Katz, H. E.; Marks, T. J. *Adv. Mater.* **2003**, *15* (1), 33. (c) Katz, H. E.; Siegrist, T.; Schön, J. H.; Kloc, C.; Batlogg, B.; Lovinger, A. J.; Johnson, J. *ChemPhysChem* **2001**, *3*, 167. (d) Malenfant, P. R. L.; Dimitrakopoulos, C. D.; Gelorme, J. D.; Kosbar, L. L.; Graham, T. O. *Appl. Phys. Lett.* **2002**, *80* (4), 2517. (e) Marks, T. J.; Facchetti, A.; Sirringhaus, H.; Friend, R. H. WO Patent 0,209,201, 2002. (f) Babel, A.; Jenekhe, S. A. *Adv. Mater.* **2002**, *145*, 371. (g) Facchetti, A.; Deng, Y.; Wang, A.; Koide, Y.; Sirringhaus, H.; Marks, T. J.; Friend, R. H. *Angew. Chem., Int. Ed.* **2000**, *39* (24), 4547. (h) Facchetti, A.; Wang, A.; Marks, T. J.; Sirringhaus, H.; Deng, Y.; Friend, R. H. *Polym. Mater. Sci. Eng.* **2000**, *83*, 290. (i) Katz, H. E.; Johnson, J.; Lovinger, A. J.; Li, W. *J. Am. Chem. Soc.* **2000**, *122*, 7787.

(3) (a) Sheraw, C. D.; Zhou, L.; Huang, J. R.; Gundlach, D. J.; Jackson, T. N.; Kane, M. G.; Hill, I. G.; Hammond, M. S.; Campi, J.; Greening, B. K.; Francl, J.; West, J. *Appl. Phys. Lett.* **2002**, *80* (6), 1088. (b) Mitschke, U.; Bauerle, P. *J. Mater. Chem.* **2000**, *10* (7), 1471. (c) Wisnieff, R. *Nature* **1998**, *394*, 225. (d) Comiskey, B.; Albert, J. D.; Yoshizawa, H.; Jacobson, J. *Nature* **1998**, *394*, 253.

(4) (a) Crone, B. K.; Dodabalapur, A.; Sarpeshkar, R.; Filas, R. W.; Lin, Y.-Y.; Bao, Z.; O'Neill, J. H.; Li, W.; Katz, H. E. *J. Appl. Phys.* **2001**, *89* (9), 5125. (b) Crone, B.; Dodabalapur, A.; Lin, Y.-Y.; Filas, R. W.; Bao, Z.; LaDuca, A.; Sarpeshkar, R.; Katz, H. E.; Li, W. *Nature* **2000**, *403*, 521. (c) Lin, Y.-Y.; Dodabalapur, A.; Sarpeshkar, R.; Bao, Z.; Li, W.; Baldwin, K.; Raju, V. R.; Katz, H. E. *Appl. Phys. Lett.* **1999**, *74* (18), 2714.

(5) (a) Bartic, C.; Palan, B.; Campitelli, A.; Borghs, G. *Sens. Actuators, B* **2002**, *83*, 115, (b) Crone, B.; Dodabalapur, A.; Gelperin, A.; Torsi, L.; Katz, H. E.; Lovinger, A. J.; Bao, Z. *Appl. Phys. Lett.* **2001**, *78* (15), 2229.

10.1021/ja035143a CCC: $25.00

recently been shown to have potential in organic transistors.[9] In a nonvolatile transistor, an added voltage is introduced between the gate and the semiconducting channel, and via charge storage, the effective gate voltage is then altered from the applied gate voltage V_g. The resulting polarization creates additional electronic states within the device, and the effective threshold voltage can be brought close to zero (or some other arbitrary value) for real-world applications where available gate voltage is limited. Previously, a memory effect in organic-based devices was only observed as a hysteresis in the current/voltage characteristics[10] or as changes in conductivity or photocurrent in two-terminal devices.[11] The advantages of a three-terminal memory device include more ready incorporation into amplifying and adaptive circuits and use as a tunable element in a multitransistor circuit block.

Unsubstituted phenylene (P)−thiophene (T) oligomers with various P:T ratios are a promising class of semiconductors; many have been employed in light-emitting diodes[12] as well as in p-channel FETs.[13,14] We have recently demonstrated a substantial memory effect in vapor-deposited 1,4-bis(5-phenyl-2-thienyl)benzene (PTPTP)- and *N*,*N*′-bis(1H,1H-perfluorooctyl)-naphthalene-1,4,5,8-tetracarboxylic diimide (F15-NTCDI)-based devices, exhibiting p- and n-type behavior, respectively, with threshold voltage shifts of up to 40 V, depending on the dielectric material and polarization conditions employed.[9] It was suggested that at least some of the charge storage must occur in the bulk of the dielectric since the incorporation into the dielectric of small amounts of additives has a significant effect on the polarization.

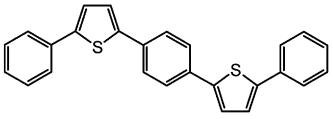

PTPTP

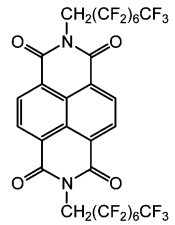

F15-NTCDI

Previous work with FETs fabricated from thiophene−phenylene oligomers functionalized with terminal *n*-hexyl groups[13] suggests that the solubilizing effect is more substantial than in all-thiophene backbones.[15] These observations raise the interesting question of whether this effect is general and whether it can lead to enhanced film-forming properties from solution.

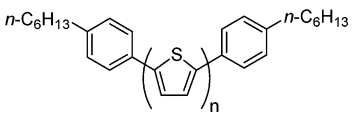

n = 1; **dH-PTP (1)**
n = 2; **dH-PTTP (2)**
n = 3; **dH-PT$_3$P (3)**
n = 4; **dH-PT$_4$P (4)**

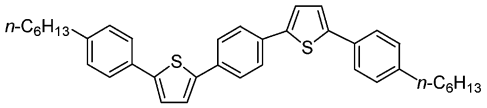

dH-PTPTP (5)

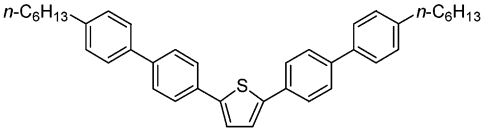

dH-PPTPP (6)

Also, the incorporation of phenylene units into the thiophene backbone results in a small lowering of the HOMO energy, and it has been shown that this lowering is accompanied by a reduction in the off current, thus increasing the device on/off ratio.[13] This effect is also apparent as a shift of the threshold voltage toward the accumulation regime.

The above observations and the questions they raise about memory function, solution processability, and device current on/off ratio tuning motivate the present study: the synthesis and characterization of a new series of *n*-hexyl-substituted thiophene−phenylene oligomers (**1**−**6**) designed for solution-processable FETs and simple nonvolatile elements. The work reported here focuses on compounds that are particularly easy to synthesize and may be readily deposited by both sublimation at moderate temperatures and casting from solution in xylenes. We demonstrate here the first example (to our knowledge) of a tunable and stable memory effect in OFETs fabricated using simple solution-casting methods. We also report more definitive experiments on a floating gate structure which support the idea that charging of the dielectric, especially near the dielectric−semiconductor interface, rather than solely at the semiconductor−metal interfaces, plays a key role.

It will be seen that compounds **1** and **2** exhibit remarkably high carrier mobilities for such small and readily prepared molecules. For compounds **2** and **6** in this series, with large threshold voltages (substantially in the accumulation regime), a large memory effect is observed on both Si/SiO_2 and ITO/GR substrates. The stability, reversibility, and tunability of this memory effect are defined, and the mechanism of charge storage

(6) (a) Otsubo, T.; Aso, Y.; Takimiya, K. *J. Mater. Chem.* **2002**, *12*, 2565. (b) Harrison, M. G.; Friend, R. H. In *Electronic Materials: The Oligomer Approach*; Müllen, K., Wegner, G., Eds.; Wiley-VCH: Weinheim, 1998; pp 515−558.

(7) (a) Afzali, A.; Breen, T. L.; Kagan, C. R. *Chem. Mater.* **2002**, *14*, 1742. (b) Halik, M.; Klauk, H.; Zschieschang, U.; Kriem, T.; Schmid, G.; Radlik, W. *Appl. Phys. Lett.* **2002**, *81* (2), 289. (c) Afzali, A.; Dimitrakopoulos, D.; Breen, T. L. *J. Am. Chem. Soc.* **2002**, *124*, 8812. (d) Kawase, T.; Sirringhaus, H.; Friend, R. H.; Shimoda, T. *Adv. Mater.* **2001**, *13* (21), 1601. (e) Sirringhaus, H.; Kawase, T.; Friend, R. H.; Shimoda, T.; Inbasekaran, M.; Wu, W.; Woo, E. P. *Science* **2000**, *290*, 2123.

(8) Sze, S. M. *Semiconductor Devices: Physics and Technology*; Wiley: New York, 1985; pp 6−7, 216−218, 507−510.

(9) Katz, H. E.; Hong, X. M.; Dodabalapur, A.; Sarpeshkar, R. *J. Appl. Phys.* **2002**, *91* (3), 1572.

(10) (a) Majumdar, H. S.; Bandyopadhyay, A.; Bolognesi, A.; Pal, A. J. *J. Appl. Phys.* **2002**, *91* (4), 2433. (b) Velu, G.; Legrand, C.; Tharaud, O.; Chapoton, A.; Remiens, D.; Horowitz, G. *Appl. Phys. Lett.* **2001**, *79* (5), 659. (c) Sentein, C.; Fiorini, C.; Lorin, A.; Nunzi, J. M. *Adv. Mater.* **1997**, *9* (10), 809.

(11) (a) Ma, L.; Liu, J.; Pyo, S.; Yang, Y. *Appl. Phys. Lett.* **2002**, *80* (3), 362. (b) Liu, C.-Y.; Bard, A. J. *Acc. Chem. Res.* **1999**, *32*, 235.

(12) (a) Yanagi, H.; Morikawa, T.; Hotta, S. *Appl. Phys. Lett.* **2002**, *81* (8), 1512. (b) Yanagi, H.; Morikawa, T.; Hotta, S.; Yase, K. *Adv. Mater.* **2001**, *13* (5), 313. (c) Dingemans, T. J.; Bacher, A.; Thelakkat, M.; Pederson, L. G.; Samulski, E. T.; Schmidt, H.-W. *Synth. Met.* **1999**, *105* (3), 171.

(13) Hong, X. M.; Katz, H. E.; Lovinger, A. J.; Wang, B.-C.; Raghavachari, K. *Chem. Mater.* **2001**, *13*, 4686.

(14) (a) Hotta, S.; Goto, M. *Adv. Mater.* **2002**, *14* (7), 498. (b) Lee, S. A.; Hotta, S.; Nakanishi, F. *J. Phys. Chem. A* **2000**, *104*, 1827. (c) Hotta, S.; Lee, S. A. *Synth. Met.* **1999**, *101*, 551.

(15) (a) Horowitz, G.; Fichou, D.; Peng, X.; Xu, Z.; Garnier, F. *Solid State Commun.* **1989**, *72*, 381. (b) Garnier, F.; Yassar, A.; Hajlaoui, R.; Horowitz, G.; Deloffre, F.; Servet, B.; Ries, S.; Alnot, P. *J. Am. Chem. Soc.* **1993**, *115*, 8716.

is further explored through devices in a "floating gate" transistor configuration. The first all-solution-processed nonvolatile devices are presented and evaluated. Finally, we propose a means to optimize memory response using dielectric materials with improved charge storage capability.

Experimental Section

Materials and General Methods. Prime grade silicon wafers with 300 nm thermally grown oxide (Process Specialties) and indium−tin-oxide (ITO)/glass spin-coated with GR-720 or GR-720P glass resin (Techneglas, Inc.) were used as device substrates. Glass resin layers were ∼2 μm. The ITO/glass substrates were polished with fine Celite and rinsed with water, methanol, and acetone before spin-coating the glass resin. The organic semiconductors were deposited by vacuum evaporation (pressures $< 10^{-5}$ Torr) and by casting from xylenes (distilled from sodium) solutions. For vacuum-evaporated films, silicon substrates were rinsed with water, methanol, and acetone before use. Trimethylsilyl functionalization of the Si/SiO_2 surface was carried out by exposing the silicon wafers to hexamethyldisilazane (HMDS) vapor in a closed container overnight. For solution depositions, a region of the substrate surface (∼1−2 cm^2) was defined using 3M Novec EGC-1700 fluorocarbon electronic coating (comparable in properties to the previously used FC-722 product) before casting.[16] Solution concentrations were 200−400 ppm, and substrate temperatures during casting were approximately 110−115 °C. The room temperature or warm solution was applied inside the defined area and allowed to evaporate, with no special care taken to avoid dust in the environment. Top-contact electrodes were deposited by evaporating gold (pressures $<10^{-5}$ Torr) or by simply painting contacts with conducting carbon paste (Structure Probe, Inc.). All devices referred to in this study employed gold electrodes unless otherwise mentioned. The additional gold electrode for "floating gate" devices was evaporated on top of the glass resin dielectric. An additional layer of glass resin was then spin-coated on this floating gate electrode before deposition of the semiconductor.

All synthetic experiments were performed under a nitrogen atmosphere using conventional Schlenk line techniques. ^{1}H NMR (400 MHz) spectra were measured with a Varian Mercury 400 (room temperature) or a Varian VXR 300 (high temperature) instrument. Thermal analyses were performed with a TA Instruments DSC 2920 differential scanning calorimeter (N_2 atmosphere) and a TA Instruments SDT 2960 simultaneous DTA-TGA instrument (10^{-2} Torr). Emission and absorption spectra were obtained with a Cary 1 ultraviolet/visible spectrometer and a PTI QM2 fluorescence instrument. Electrical measurements were performed using a home-built coaxial probe station and a Hewlett-Packard 4155A semiconductor parametric analyzer. Fabricated devices were analyzed in situ by X-ray film diffractometry (XRD), using standard $\theta-2\theta$ scanning techniques [calibration to Si(100)], with Cu Kα radiation and a monochromator, and by scanning electron microscopy (SEM), using a Hitachi S4500 FE microscope. The reagents 5,5′-bis(tri-*n*-butylstannyl)-2,2′-bithiophene,[17] 2,5-bis(tri-*n*-butylstannyl)-thiophene,[17] and 5,5′-dibromo-2,2′-bithiophene[18] were prepared according to known procedures. General procedures for preparation of tributylstannyl derivatives[19] were employed with slight modifications for new compounds **9** and **10**. The reagent 1,4-bis(2-thienyl)benzene was prepared via the Grignard coupling[20] of 2-thienylmagnesium bromide with 1,4-diiodobenzene. Alternatively, it can be synthesized by transition-metal-catalyzed coupling of 2-thienylzinc chloride with 1,4-dibromobenzene.[21,22] The reagent 1,4-bis(5-bromo-2-thienyl)benzene was synthesized by bromination of 1,4-bis(2-thienyl)benzene in DMF with *N*-bromosuccinimide,[18,21] and 2,5-bis(4-bromophenyl)-thiophene was synthesized by the Pd(0)-catalyzed coupling of 2,5-dibromothiophene with 4-bromophenylboronic acid according to a known procedure.[23] Other chemicals and solvents are commercially available.

Preparation of 2-(Tri-*n*-butylstannyl)-5-(4-*n*-hexylphenyl)thiophene (9) and 1-(Tri-*n*-butylstannyl)-4-*n*-hexylbenzene (10). To a solution of 5-(4-*n*-hexylphenyl)thiophene (1.52 g, 6.22 mmol) in dry THF (30 mL) in a bath at −78 °C was slowly added a hexanes solution of *n*-BuLi (3.9 mL, 6.2 mmol). After 1 h of stirring at this temperature, tri-*n*-butyltin chloride (2.0 g, 6.2 mmol) was added, and the reaction mixture was allowed to warm slowly to room temperature and stir overnight. Hexane (50 mL) was then added. The reaction mixture was washed with 5% $NaHCO_3$ (20 mL) and water (2 × 20 mL), dried over $MgSO_4$, filtered, and concentrated in vacuo to give 3.2 g of clear, light yellow liquid (97%). The same procedure was followed for compound **10**, and both **9** and **10** were used as crude materials in subsequent reactions. Compound **9**: ^{1}H NMR ($CDCl_3$) δ 7.51 (d, 2H, ^3J = 8.2 Hz), 7.37 (d, 1H, ^3J = 3.4 Hz), 7.15 (d, 2H), 7.10 (d, 1H), 2.58 (t, 2H, ^3J = 8.0 Hz), 1.59−1.53 (m, 8H), 1.36−1.27 (m, 12H), 1.10 (t, 6H, ^3J = 8.4 Hz), 0.91−0.87 (m, 12H). HRMS (EI, 70 eV) *m*/*z*: calcd for $C_{28}H_{46}SSn$, 534.2341; found, 534.5131. Compound **10**: ^{1}H NMR ($CDCl_3$) δ 7.39 (d, 2H, ^3J = 7.6 Hz), 7.14 (d, 2H), 2.57 (t, 2H, ^3J = 7.8 Hz), 1.62−1.48 (m, 12H), 1.03 (t, 6H, ^3J = 8.0 Hz), 0.91−0.86 (m, 12H). HRMS (EI, 70 eV) *m*/*z*: (M^+) calcd for $C_{24}H_{44}Sn$, 452.2465; found, 451.2426.

Preparation of 2-(4-*n*-Hexylphenyl)thiophene (8). A mixture of 4-bromo-*n*-hexylbenzene (**7**; 5.68 g, 23.5 mmol), 2-tri-*n*-butylstannylthiophene (8.84 g, 23.7 mmol), and tetrakis(triphenylphosphine)-palladium(0) (0.4 g, 0.4 mmol) in dry DMF (90 mL) was heated under nitrogen at 90 °C overnight. After the reaction was cooled to room temperature, water (250 mL) and hexane (100 mL) were added. The organic layer was separated, and the aqueous layer was extracted with hexane (2 × 100 mL). The organic layers were combined, washed with water (2 × 100 mL), dried over $MgSO_4$, filtered, and concentrated in vacuo to give a clear orange liquid. After purification by column chromatography on silica gel (hexane), 2-(4-*n*-hexylphenyl)thiophene (**8**) is obtained as a clear, colorless liquid: ^{1}H NMR ($CDCl_3$) δ 7.50 (d, 2H, ^3J = 8.0 Hz), 7.25 (d, 1H, ^3J = 3.6 Hz), 7.23 (d, 1H, ^3J = 5.2 Hz), 7.17 (d, 2H), 7.05 (dd, 1H), 2.59 (t, 2H, ^3J = 8.0 Hz), 1.63−1.57 (m, 2H), 1.36−1.28 (m, 6H), 0.87 (t, 3H, ^3J = 7.2 Hz). HRMS (EI, 70 eV) *m*/*z*: (M^+) calcd for $C_{16}H_{20}S$, 244.1286; found, 244.1245.

Preparation of 2,5-Bis(4-*n*-hexylphenyl)thiophene (dH-PTP, 1). A mixture of 4-bromo-*n*-hexylbenzene (**7**; 3.01 g, 12.5 mmol), 2,5-bis(tri-*n*-butylstannyl)thiophene (3.81 g, 5.75 mmol), and tetrakis-(triphenylphosphine)palladium(0) (0.14 g, 0.12 mmol) in dry dimethylformamide (20 mL) was heated under nitrogen at 80 °C overnight. The reaction mixture was then poured into water (50 mL) and extracted with hexanes (3 × 30 mL). The organic phase was then washed with water (2 × 30 mL), dried over $MgSO_4$, filtered, and concentrated in vacuo to give a pale yellow solid **1**, which was recrystallized from hexane (1.44 g, 62%): mp 144 °C; ^{1}H NMR ($CDCl_3$) δ 7.52 (d, 4H, ^3J = 8.0 Hz), 7.21 (s, 2H), 7.17 (d, 4H), 2.59 (t, 4H, ^3J = 7.6 Hz), 1.63−1.57 (m, 4H), 1.34−1.27 (m, 12H), 0.87 (t, 6H, ^3J = 6.6 Hz). Anal. Calcd for $C_{28}H_{36}S$: C, 83.11; H, 8.97. Found: C, 82.61; H, 8.70.

Preparation of 5,5′-Bis(4-*n*-hexylphenyl)-2,2′-bithiophene (dH-PTTP, 2). A mixture of 4-bromo-*n*-hexylbenzene (**7**; 1.21 g, 5.02 mmol), 5,5′-bis(tri-*n*-butylstannyl)-2,2′-dithiophene (1.69 g, 2.27 mmol),

(16) Katz, H. E. U.S. Patent 6,403,397, 2002.
(17) Wei, Y.; Yang, Y.; Yeh, J.-M. *Chem. Mater.* **1996**, *8*, 2659.
(18) Bäuerle, P.; Würthner, F.; Götz, G.; Effenberger, F. *Synthesis* **1993**, *11*, 1099−1103.
(19) Peters, D.; Hörnfeldt, A.-B.; Gronowitz, S. *J. Heterocycl. Chem.* **1991**, *28*, 1613−1617.
(20) Tamao, K.; Kodama, S.; Nakajima, I.; Kumada, M.; Minato, A.; Suzuki, K. *Tetrahedron* **1982**, *38* (22), 3347−3354.
(21) Pelter, A.; Jenkins, I.; Jones, D. E. *Tetrahedron* **1997**, *53* (30), 10357−10400.
(22) Sarker, H.; Gofer, Y.; Killian, J. G.; Poehler, T. O.; Searson, P. C. *Synth. Met.* **1998**, *97*, 1−6.
(23) Alo, B. I.; Kandil, A.; Patil, P. A.; Sharp, M. J.; Siddiqui, M. A.; Snieckus, V.; Josephy, P. D. *J. Org. Chem.* **1991**, *56* (12), 3763−3768.

and $Pd(PPh_3)_4$ (0.07 g, 0.06 mmol) in DMF (35 mL) was heated under nitrogen at 80 °C overnight. The dark yellow precipitate was then collected, washed several times with methanol, diethyl ether, and hexane, and dried under reduced pressure (0.75 g, 68%). The crude solid was recrystallized from toluene/hexane to afford an analytically pure yellow-orange solid **2**: mp 232 °C; ^{1}H NMR ($CDCl_3$) δ 7.50 (d, 4H, ^3J = 8.0 Hz), 7.19−7.17 (m, 6H), 7.12 (d, 2H, ^3J = 3.6 Hz), 2.60 (t, 4H, ^3J = 7.6 Hz), 1.62−1.58 (m, 4H), 1.36−1.27 (m, 12H), 0.87 (t, 6H, ^3J = 6.4 Hz). Anal. Calcd for $C_{32}H_{38}S_2$: C, 78.96; H, 7.87. Found: C, 79.06; H, 7.80.

Preparation of 5,5″-Bis(4-*n*-hexylphenyl)-2,2′:5′,2″-terthiophene (dH-PT$_3$P, 3). A mixture of 2,5-dibromothiophene (0.39 g, 1.6 mmol), 2-(tri-*n*-butylstannyl)-5-(4-*n*-hexylphenyl)thiophene (**9**; 3.97 mmol), and $Pd(PPh_3)_4$ (0.07 g, 0.06 mmol) in DMF (15 mL) was heated under nitrogen at 90 °C overnight. The precipitate was then collected, washed several times with methanol, acetone, diethyl ether, and hexanes, and dried under reduced pressure (0.70 g, 76%). The crude product was then recrystallized from toluene/1,1,2-trichloroethane to give an analytically pure light orange solid **3**: mp 284 °C; ^{1}H NMR ($C_2D_2Cl_4$, 80 °C) δ 7.53 (d, 4H, ^3J = 8.4 Hz), 7.23−7.21 (m, 6H), 7.17 (s, 2H), 7.13 (s, 2H), 2.65 (t, 4H, ^3J = 7.6 Hz), 1.70−1.63 (m, 4H), 1.41−1.34 (m, 12H), 0.93 (t, 6H, ^3J = 6.4 Hz). Anal. Calcd for $C_{36}H_{40}S_3$: C, 76.00; H, 7.09. Found: C, 75.88; H, 6.88.

Preparation of 5,5‴-Bis(4-*n*-hexylphenyl)-2,2′:5′,2″:5″,2‴-quaterthiophene (dH-PT$_4$P, 4). A mixture of 2-(tri-*n*-butylstannyl)-5-(4-*n*-hexylphenyl)thiophene (**9**) (4.49 mmol), 5,5′-dibromo-2,2′-bithiophene (0.58 g, 1.79 mmol), and $Pd(PPh_3)_4$ (0.08 g, 0.07 mmol) in DMF (30 mL) was heated under nitrogen at 90 °C overnight. The precipitate was then collected, washed several times with methanol, diethyl ether, and hexanes, and dried under reduced pressure (0.87 g, 75%). The crude product was then recrystallized from toluene/1,1,2-trichloroethane to give an analytically pure dark orange solid **4**: mp 348 °C; ^{1}H NMR ($C_2D_2Cl_4$, 100 °C) δ 7.54 (d, 4H, ^3J = 7.6 Hz), 7.24−7.22 (m, 6H), 7.18 (s, 2H), 7.14 (s, 4H), 2.67 (t, 4H, ^3J = 7.6 Hz), 1.73−1.66 (m, 4H), 1.42−1.37 (m, 12H), 0.94 (t, 6H, ^3J = 6.4 Hz). Anal. Calcd for $C_{40}H_{42}S_4$: C, 73.80; H, 6.50. Found: C, 73.43; H, 6.29.

Preparation of 1,4-Bis[5-(4-*n*-hexylphenyl)-2-thienyl]benzene (dH-PTPTP, 5). A mixture of 1-(tri-*n*-butylstannyl)-4-*n*-hexylbenzene (**10**) (2.6 mmol), 1,4-bis(5-bromo-2-thienyl)benzene (0.40 g, 1.0 mmol), and $Pd(PPh_3)_4$ (0.06 g, 0.05 mmol) in dry DMF (20 mL) was heated under nitrogen at 90 °C overnight. The precipitate was then collected and washed several times with methanol, ether, and hexane to give a yellow-brown solid (0.46 g, 82%), which was then recrystallized from toluene/1,1,2-trichloroethane: mp 324 °C; ^{1}H NMR ($C_2D_2Cl_4$, 100 °C): δ 7.67 (s, 4H), 7.57 (d, 4H, ^3J = 7.6 Hz), 7.33 (d, 2H, ^3J = 3.2 Hz), 7.28 (d, 2H), 7.24 (d, 4H), 2.67 (t, 4H, ^3J = 7.6 Hz), 1.73−1.66 (m, 4H), 1.43−1.36 (m, 12H), 0.94 (t, 6H, ^3J = 6.0 Hz). Anal. Calcd for $C_{38}H_{42}S_2$: C, 81.09; H, 7.52. Found: C, 80.97; H, 7.42.

Preparation of 2,5-Bis[4(4′-*n*-hexylphenyl)phenyl]thiophene (dH-PPTPP, 6). A mixture of 1-(tri-*n*-butylstannyl)-4-*n*-hexylbenzene (**10**) (5.1 mmol), 2,5-bis(4-bromophenyl)thiophene (0.80 g, 2.03 mmol), and $Pd(PPh_3)_4$ (0.1 g, 0.08 mmol) in dry DMF (35 mL) was heated under nitrogen at 90 °C overnight. After the reaction mixture had cooled, it was filtered, and the precipitate was washed several times with methanol, ether, and hexane to give a tan-yellow solid (0.69 g, 69%), which was recrystallized from toluene/1,1,2-trichloroethane: mp > 360 °C; ^{1}H NMR ($C_2D_2Cl_4$, 100 °C) δ 7.72 (d, 4H, ^3J = 8.4 Hz), 7.65 (d, 4H), 7.57 (d, 4H, ^3J = 7.6 Hz), 7.36 (s, 2H), 7.29 (d, 4H), 2.70 (t, 4H, ^3J = 7.6 Hz), 1.75−1.68 (m, 4H), 1.43−1.37 (m, 12H), 0.95 (t, 6H, ^3J = 6.4 Hz). HRMS (EI, 70 eV) *m*/*z* (M^+): calcd for $C_{40}H_{44}S$, 556.3154; found, 556.3164.

Results and Discussion

Synthetic Strategies. Structures **1**−**6** were targeted because they were anticipated to combine the high mobility characteristics typically exhibited by thiophene−phenylene oligomers[1,9,13] with the improved solubility/film processability and close packing tendencies associated with α,ω alkyl chain substitution.[15b,24] Straightforward syntheses, thermal stability, and solution processability make these oligomers very attractive candidates for low-cost molecular electronics applications. The phenylene−thiophene oligomers **1**−**6** were prepared via palladium(0)-catalyzed coupling of the appropriate bromo derivatives with the corresponding tri-*n*-butylstannyl derivatives, as shown in Scheme 1. The smallest oligomers **1** and **2** require only one and two steps, respectively. For all coupling reactions, tri-*n*-butylstannyl derivatives were not purified before use in subsequent reactions. All of oligomers **1**−**6** are readily purified by recrystallization rather than high-vacuum sublimation and can be stored for at least several months in air with no apparent decomposition or discoloration.

Optical absorption and emission maxima, extinction coefficients, optical band gaps, melting points, and thermal transition temperatures (DSC) for compounds **1**−**6** are summarized in Table 1. The absorption and emission characteristics, as expected, correlate very well with those of the analogous unsubstituted systems.[14] The two largest band gaps, 3.22 and 3.16 eV, correspond to compounds **1** and **6**, which have the largest ratios of phenylene to thiophene units in the backbone structure. Presumably **1** and **6** exhibit additional twisting of the conjugated backbone due to the phenylene rings, which effectively decreases the conjugation.

Differential scanning calorimetry reveals reversible melting features for oligomers **1**−**6**, with each oligomer exhibiting one or more thermal transitions before melting. Figure 1 shows the DSC trace for compound **2**, which is typical of the series. This compound exhibits three liquid crystalline transitions: an S_F/S_B to S_C followed by an S_A/nematic phase transition. Correlation between film quality, LC phase, and device performance for films of **1**−**6** is currently under investigation. In addition to reversible melting features, clean and quantitative sublimation is observed in thermogravimetric analysis of compounds **1**−**5**. Compound **6**, however, decomposes to some extent upon sublimation, leaving about 10% residue by weight. The TGA plots for **1**−**6** are compared in Figure 2. Interestingly, for compounds with a highly exothermic LC transition (**4**, **5**, and **6**) before melting, sublimation (as observed by TGA) is complete at temperatures much lower than the melting point. Compounds **4** and **5** (mp's 358 and 324 °C, respectively) completely sublime before 330 and 275 °C, respectively, while compounds **1**, **2**, and **3** (mp's 144, 232, and 284 °C, respectively) are not fully sublimed until temperatures 10−35° *higher* than their respective melting points.

Film Growth and Characterization. Without exception, the smoothest and most continuous films of **1**−**6** from solution are obtained by casting from xylenes solutions. Other solvents (benzene, toluene, chlorobenzene, choroform, 1,2,5-trichlorobenzene, 1,1,2,2-tetrachloroethane, and 1,2-dichloroethane) typically result in uneven films with areas of heavy deposition, distinguishable by eye or optical microscopy as islands of crystalline material, and areas of very light or no deposition. The occasional smooth film obtained from casting with one of these solvents is not easily reproducible. All solvents were explored under a range of deposition temperatures, from substantially below the boiling point of the solvent to just above

(24) Fichou, D. *J. Mater. Chem.* **2000**, *10*, 571.

Scheme 1. Synthetic Scheme for Thiophene−Phenylene Oligomers **1**−**6**[a]

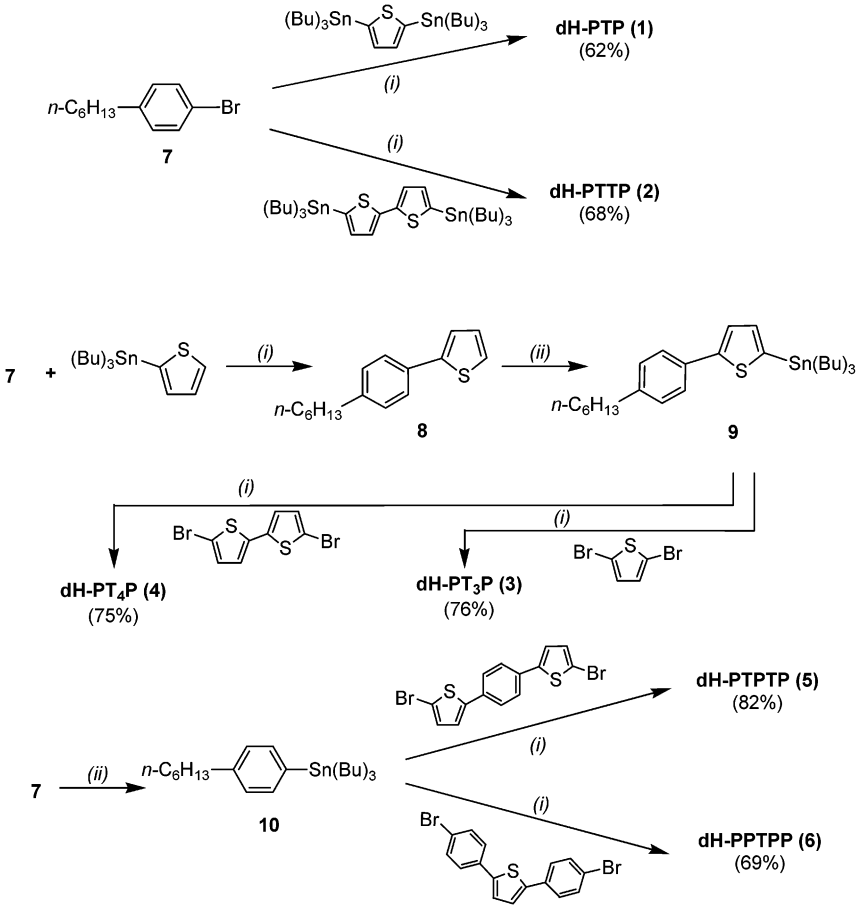

[a] (i) $Pd(PPh_3)_4$, DMF, 80−90 °C. (ii) (1) BuLi, THF, −78 °C, (2) Bu_3SnCl.

Table 1. Optical Absorption and Emission Maxima in THF Solution, Extinction Coefficients, Optical Band Gaps, Capillary Tube Melting Points, and DSC Transition Temperatures (2nd Heating Cycle) of Phenylene−Thiophene Oligomers **1**−**6**

compound	λ_{abs} (nm)	log ϵ	λ_{em}[a] (nm)	E_g (eV)	mp (°C)	T_{DSC}[b] (°C)
dH-PTP (**1**)	366	4.51	385	3.22	144	92, 150*
dH-PTTP (**2**)	373	4.60	436, 460*	2.97	232	139, 150, 235*, 239
dH-PT_3P (**3**)	408	4.71	472*, 503	2.77	284	278*, 295
dH-PT_4P (**4**)	432	4.73	498*, 536	2.62	358	328*, 356, 362
dH-PTPTP (**5**)	378	4.78	432*, 458	3.01	324	83, 267*, 323, 328
dH-PPTPP (**6**)	356	4.16	414, 437*	3.16	>360	299*, 365, 369

[a] Absolute maximum indicated by asterisk. [b] Largest thermal transition indicated by asterisk.

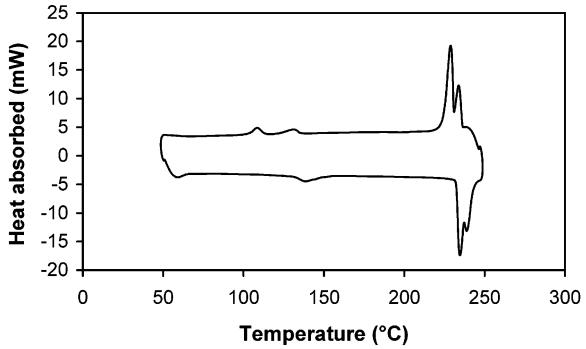

Figure 1. Differential scanning calorimetry trace (second cycle) for dH-PTTP (**2**) showing reversible melting and liquid crystalline transitions (ramp rate, 10 °C/min).

it. Higher-boiling solvents typically produce smoother films at temperatures in the range of 5−30 °C below their boiling points. All solution-cast films characterized in this study were cast from xylenes solutions at a substrate temperature of 115 ± 10 °C on ITO/glass resin, due to the high reproducibility of film quality under these conditions. As an example, the FET performance of **2** is highly dependent on casting temperature; devices cast at substrate temperatures outside of a range of ∼110−120 °C showed significantly lower carrier mobilities. The capability of casting highly reproducible, smooth, and continuous films from a non-chlorinated solvent is a significant step toward low-cost and low-toxicity solution fabrication techniques. The mechanism by which an oligothiophene film forms on a substrate from the overlying solution is poorly understood and is under investigation.

The phenylene−thiophene oligomers prepared in this study all yield highly ordered films on Si/SiO_2 and ITO/GR substrates, both by evaporation under high vacuum and by deposition from cast xylenes solutions, as assessed by X-ray diffraction. The observed intense reflections and calculated interplanar *d* spacings for solution-cast and vacuum-evaporated films of oligomers **1**−**6** are summarized in Table 2. In all films, the first-order reflection is very intense, and many films exhibit well-resolved higher-order reflections as well, indicating well-ordered, layered microstructures. Vacuum deposition at a substrate temperature of 50 °C enhances XRD peak sharpness, but since there is not a substantial difference in device performance, the substrate temperature during growth was not further optimized in this

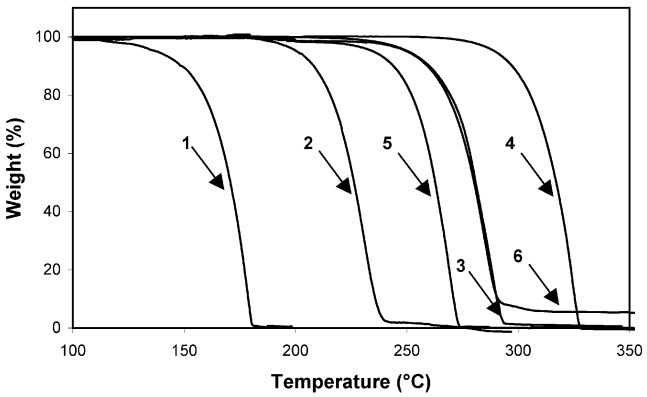

Figure 2. Thermogravimetric analysis data (10^{-2} Torr, 1.5 °C/min) for phenylene−thiophene oligomers **1**−**6**.

Table 2. X-ray Diffraction Data for Vacuum-Evaporated and Solution-Cast Films of Phenylene−Thiophene Oligomers: Major Reflections and Derived Interplanar Distances

	vacuum-deposited films (25 °C substrate temperature)		solution-cast films (xylenes solution, 110–115 °C)	
compound	*d* (Å)	other observable reflections (order)	*d* (Å)	other observable reflections (order)
dH-PTP (**1**)	25	none	25	none
dH-PTTP (**2**)	30	2, 3, 4, 5, 6[b]	30 (26)[a]	3, 4, 5, 6[b]
dH-PT_3P (**3**)	35	2	31	2 (weak)
dH-PT_4P (**4**)	39	2	37	2
dH-PTPTP (**5**)	35	2, 4 (weak), 6 (weak)	33	2 (weak)
dH-PPTPP (**6**)	38	2	35	none

[a] Peaks corresponding to a second phase are also observed. [b] Scans did not extend higher than 6th order peaks.

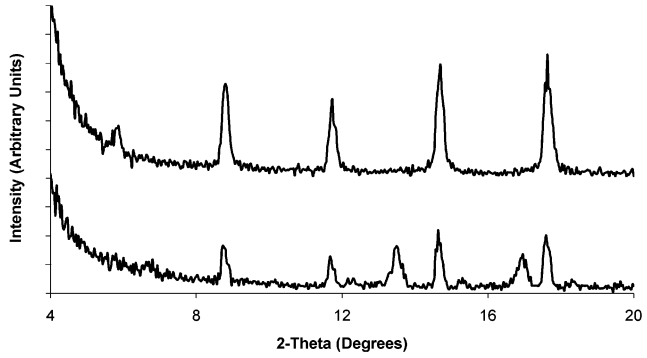

Figure 3. X-ray diffraction $\theta-2\theta$ scans of solution-cast (from xylenes solution, 110−115 °C; bottom) and vacuum-evaporated (ambient temperature; top) films of dH-PTTP (**2**) on Si/SiO_2 substrates.

study. Pretreatment of the silicon substrates with HMDS vapor to create lipophilic monolayer coatings has negligible effects on the XRD results. Figure 3 compares $\theta-2\theta$ diffraction scans of solution-cast (bottom) versus vacuum-evaporated (top) films of **2**. Unlike films of the other oligomers, films of **2** contain two major crystallite orientations or phases when cast from solution. Because of the non-negligible difference in the measured *d* spacings (4 Å) from the first (low-angle) reflections (30 and 26 Å), it appears likely that these two distinct lattice spacings correspond to distinct growth orientations or polymorphs of compound **2**. This phenomenon has been observed in various substituted oligothiophenes as well,[24] including the all-thiophene analogue of **2**, α,ω-dihexylquaterthiophene.[25]

Previous diffraction studies on films of analogous phenylene−thiophene oligomers without α,ω-alkyl substituents indicate that smaller oligomers (<5 thiophene or phenyl rings) favor vertical molecular alignment (long molecular axis roughly perpendicular to the substrate surface) over parallel alignment (long molecular axis roughly parallel to the substrate surface) when compared to larger oligomers (≥5 rings) deposited under identical conditions (casting from methylene chloride solution or evaporating at $\sim10^{-6}$ Torr and a growth rate of 1−2 Å/sec).[26] Previous work also showed that exclusively vertical molecular alignment (no detectable presence of reflections corresponding to parallel alignment structures) can be achieved for some compounds only under higher vacuum ($\sim10^{-9}$ Torr) and at extremely low film deposition rates (<0.01 Å/sec).[26] As seen in Table 2, we observe for **1**−**6** that vertical molecular alignment is predominant for all films grown by either solution or vacuum techniques (deposition rates of <3 Å/sec and pressures < 10^{-6} Torr) but that, generally, the *longer* oligomers exhibit *smaller* apparent tilt angles of the molecular long axes with respect to the substrate normal, contrary to what was observed for the unsubstituted analogues.[26] That is, the present experimental interplanar *d* spacings correlate very well with the calculated long molecular axis lengths of the oligomers, taking into account reasonable tilt angles. Simple addition of the molecular lengths of the analogous unsubstituted oligomers (13, 17, 21, 24, 21, and 22 Å, in analogous order to **1**−**6**)[26] and the length estimated for two hexyl chains (~9.3 Å each)[15b] affords values 2 to 6 Å larger than the experimentally determined *d* spacings for vacuum-evaporated films of **2**−**6** shown in Table 2. Assuming molecular packing motifs similar to those of the unsubstituted oligomers,[26] this implies tilt angles of approximately 25−40° from the substrate normal (except for the shortest oligomers **1** and **2**, with apparent tilt angles of 50−60°), with solution-cast films having slightly larger apparent tilt angles (10−15° greater) than evaporated films of the same compound (except for the shortest, **1**, for which they are identical). The large difference in growth rate between solution-casting and vacuum evaporation may give rise to different growth directions or packing motifs, which is a reasonable explanation for the larger apparent tilt angles seen in solution-cast films. As noted above, the growth rate has a significant effect on molecular alignment for the unsubstituted phenylene−thiophene oligomers.[26]

Scanning electron microscopy (SEM) reveals very smooth morphologies for evaporated films of all phenylene−thiophene compounds **2**−**6** grown both at ambient temperature and at 50 °C (the lower-melting **1** was not examined by SEM). Much greater variation in morphology is observed for solution-cast films, with the larger oligomers **3**−**6** displaying overlapping crystallites having dimensions as large as several tens of micrometers. The smaller molecule **2**, however, adopts quite a different film morphology (as cast from solution) from the others; it is much more smooth and has much smaller features. Figure 4 compares typical micrographs of **2** and **3** to illustrate this difference. In general, the interconnectedness of crystallites in the solution-cast films imaged by SEM combined with the high order of crystallinity and vertical molecular alignment seen in the XRD provide strong support for the efficient hole-transporting capabilities of **1**−**6**.

(25) Garnier, F.; Hajlaoui, R.; El Kassmi, A.; Horowitz, G.; Laigre, L.; Porzio, W.; Armanini, M.; Provasoli, F. *Chem. Mater.* **1998**, *10*, 3334.

(26) Hotta, S.; Ichino, Y.; Yoshida, Y.; Yoshida, M. *J. Phys. Chem. B* **2000**, *104*, 10316.

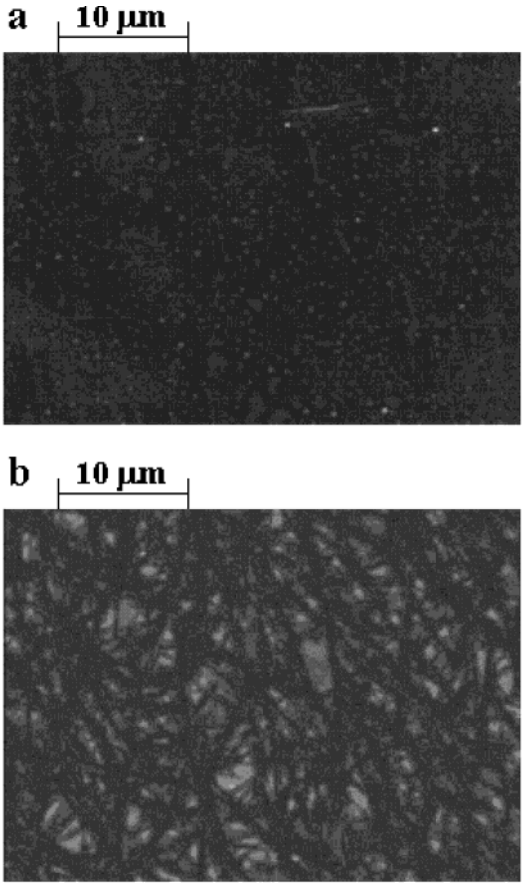

Figure 4. Scanning electron micrographs of films cast from xylenes solution on Si/SiO_2 at 110−115 °C of (a) dH-PTTP (**2**) (400 ppm concentration) and (b) dH-PT_3P (**3**) (300 ppm concentration).

Transistor and Nonvolatile Memory Characteristics. In p-channel operation, compounds **2**−**6** display hole mobilities between 0.01 and 0.09 cm^2/Vs as vacuum-evaporated films (on Si/SiO_2) and between 0.001 and 0.03 cm^2/Vs as solution-cast films (on ITO/GR). The response of compound **1** varies substantially from device to device and shows a significant mobility as an evaporated film only on HMDS-treated SiO_2. These data are summarized in Table 3 and shown for dH-PTTP (**2**) in Figure 5. Pretreatment of substrates with HMDS before vacuum evaporation has negligible effects on the FET response of **2**, **4**, and **6** but increases the current on/off ratios of room-temperature-evaporated films of **3** and **5** by 1 or 2 orders of magnitude. In several cases, devices in fact display greater performance on untreated silicon substrates than on HMDS-treated ones (refer to Table 3). Regardless of the surface pretreatment, FET characteristics for both evaporated and solution-cast films are highly reproducible, and on/off ratios of 10^4 and higher are readily obtainable. It is particularly notable that useful mobilities, on/off ratios, and resistance to doping (as indicated by off currents of $\sim 10^{-10}$ A) are obtained from **1** and **2**, which can be synthesized in so few steps from readily available starting materials. Compound **2** in particular is the most reliable thiophene derivative yet identified for rapidly producing an undoped, air-stable, semiconducting film from solution. Furthermore, vacuum sublimation is *not* required to purify these two semiconductors to a level that exhibits large current on/off ratios.

Solution-cast films on ITO/GR substrates were used for all of the following memory effect experiments; Si/SiO_2 devices are briefly compared later. Writing voltages V_w were applied at the gate with a common voltage at the source and drain. Threshold voltages V_t were calculated from the plot of $I_d^{0.5}$ versus V_g, where the *x*-intercept of the linear portion of the plot is V_t.[9] Before and after the writing voltages were applied, the FET characteristics were measured and the characteristics compared. Both dH-PTTP (**2**) and dH-PPTPP (**6**) show a substantial memory effect; high initial device turn-on voltages for **2** and **6** can be brought from accumulation mode turn-on to zero or depletion mode by applying a writing voltage. Of the two, the better-behaved system is dH-PTTP (**2**) because of the reversibility and predictability of the effects of the applied writing voltage. Figure 6 shows representative current−voltage plots for a solution-cast device of dH-PTTP (**2**) (ITO/GR with top contact Au electrodes) before and after the application of a writing voltage of +100 V for 1.0 min. The plots include only the current−voltage curves for gate values of 0 V, −20 V, and −40 V, to show more clearly the magnitude of the effect of writing.

An informative measure of the memory effect is the ratio of the maximum current after writing to the maximum current before writing, at a gate voltage of −20 V (I_{max}, where $V_{sd} = -100$ V and $V_g = -20$ V). In accord with a mechanism in which the stored charge from writing affects the accumulation of majority carriers in the channel by prefilling traps (discussed below),[9] the largest effects in the current−voltage characteristics are observed at *lower* V_g values, where traps have a greater effect. The ratio of maximum current ($V_{sd} = -100$ V, $V_g = -20$ V) after writing to that before writing is about 12 for the device shown in Figure 6, and the turn-on voltage shift is from about −50 V to about −30 V. Typical current ratios for ITO/GR devices fabricated from solution-cast **2** for this writing voltage and time are in the range of 5−15, although ratios as high as 25 are sometimes observed. Typically these ratios drop upon measurement, and after just a few cycles, where a cycle is defined as a sweep of V_{sd} from 0 to −100 V for V_g values of 0, −20, −40, −60, −80, and −100 V, the ratio of I_{max} after writing to before writing drops by more than 50%, although it is still easily detectable. If, however, lower voltages are used in measuring the device between writing voltages, the effect persists much longer. If V_{sd} and V_g are each swept only to −40 V, for example, the ratio of maximum currents at $V_g = -20$ V (now for $V_{sd} = -40$ V) after writing to before writing remains within 75% of its initial value after more than 15 cycles.

The memory effect (measured in terms of the ratio of maximum currents at $V_g = -20$ V before and after writing) can be tuned by writing at various voltages and for various times. It can also be selectively erased and restored multiple times without a change in magnitude and without breakdown of the device. Figure 7 shows an example of this tuning for an ITO/GR device with solution-cast **2**. Taking the original ratio as 1.0 (effectively, application of $V_w = 0$ V) and then applying some positive writing voltage, we can tune the current for smaller or larger effects and subsequently erase it by writing with the appropriate negative (opposite) voltage. In this example, a writing voltage of +50 V applied for 10 min increases the current ratio to about 8, as does a writing voltage of +100 V applied for 3 min. The negative writing voltages applied to

Table 3. FET Mobilities and On/Off Ratios for Vacuum-Evaporated and Solution-Deposited Phenylene−Thiophene Semiconductor Films

	solution-cast films[a] (xylenes, 110–115 °C)		vacuum-deposited films[b]			
			room temperature		50 °C	
compd	mobility (cm^2/Vs)	I_{ON}/I_{OFF}	mobility (cm^2/Vs)	I_{ON}/I_{OFF}	mobility (cm^2/Vs)	I_{ON}/I_{OFF}
1	10^{-5}	60	$\sim10^{-5}$ (0.01)	30 (2500)	$\sim10^{-4}$ (0.01)	200 (3000)
2	0.02 [0.006]	2×10^4 [3×10^3]	0.07 (0.09)	10^5 (10^5)	0.09 (0.09)	4×10^4 (1.5×10^5)
3	0.004 [3×10^{-4}]	100 [10]	0.054 (0.028)	7700 (2×10^4)	0.054 (0.028)	6000 (2800)
4	0.028 [10^{-3}]	1000 [10]	0.09 (0.054)	900 (3500)	0.07 (0.09)	1400 (1100)
5	0.01	1700	0.054 (0.054)	900 (4×10^4)	0.028 (0.054)	5×10^4 (6×10^4)
6	0.001	600	0.001 (7×10^{-4})	1100 (600)	0.018 (0.018)	10^4 (1.5×10^4)

[a] Values in brackets refer to all-solution devices fabricated on ITO with spin-coated glass resin, solution-cast semiconductors, and painted graphite electrodes. [b] Values in parentheses refer to devices on silicon substrates that were treated with hexamethyldisilazane (HMDS) before film growth.

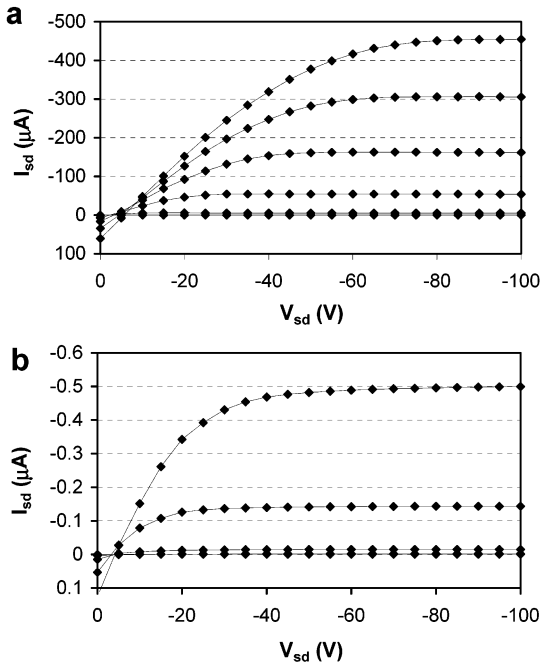

Figure 5. Current−voltage characteristics for devices with evaporated Au top-contact electrodes and dH-PTTP (**2**) films: (a) vacuum-deposited onto Si/SiO_2 and (b) cast from 400 ppm xylene solution at 115 °C onto ITO/GR. Gate voltages are 0 to −100 V in increments of 20 V, bottom to top (on bottom plot V_g 0 to −40 V all overlap at 0 V).

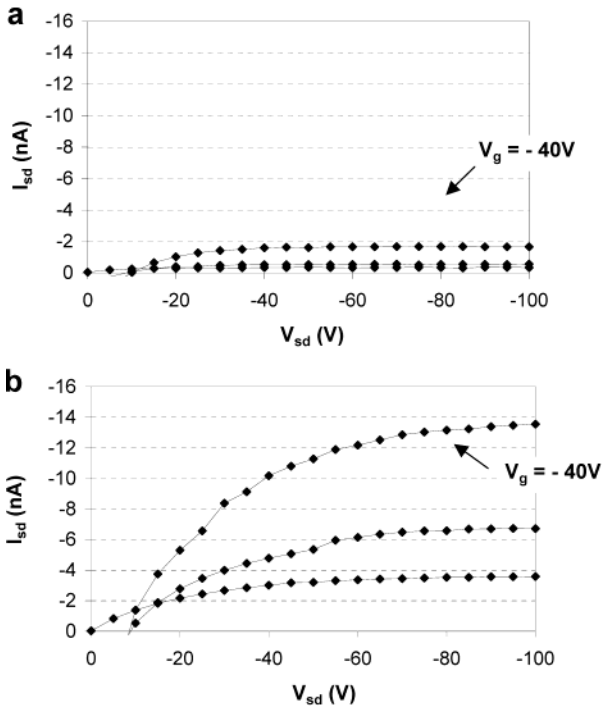

Figure 6. Current−voltage characteristics for solution-cast dH-PTTP (**2**) on ITO/GR with top-contact evaporated Au electrodes: (a) before and (b) after writing with $V_w = +100$ V for 1.0 min. Gate voltages are 0, −20, and −40 V, from bottom to top.

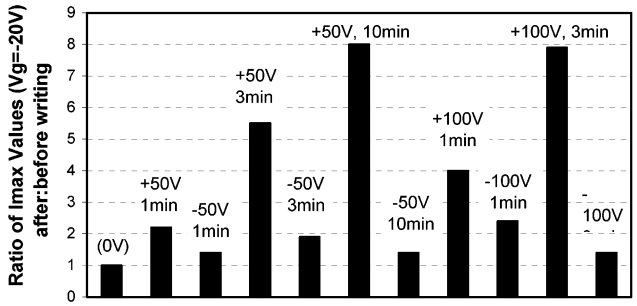

Figure 7. Histogram showing the tunability of the memory effect for a solution-cast dH-PTTP (**2**)-based device on ITO/GR with various applied voltages and times. Each bar represents the ratio of the maximum current at $V_g = -20$ V after the indicated writing voltage is applied to the same maximum current before the writing voltage is applied.

"erase" the memory effect, or remove the stored charge, consistently bring the maximum current value (at $V_g = -20$ V) to less than 2.5 times its value before writing. By slightly increasing the writing time for the opposite V_w, we can bring the maximum current to within less than 1.2 times its original value.

In comparison with ITO/GR, devices of Si/SiO_2 with solution-cast **2** exhibit a much larger ratio of maximum currents, but the effect disappears almost instantaneously, even before the first cycle is complete. Thus, the ratio of maximum currents ($V_{sd} = -100$ V) must be compared at $V_g = 0$ V in order to detect a large effect, and after one full cycle of measurements up to $V_g = -100$ V, the effect is essentially undetectable. Ratios are typically in the range of 225−500, but values as high as 650 are observed. Glass resin has a much higher charge storage capability than SiO_2; the observed difference in the effect is as expected.[9] Optimization of the dielectric should enable far larger and more stable writing effects.

A physical mechanism for the memory effect has been suggested previously.[9] Briefly, holding a voltage across the gate dielectric ("writing") causes the injection of static charge somewhere between the semiconductor and gate electrode, either in the bulk of the dielectric and/or at one or both dielectric interfaces. The charge may be in the form of isolated monopoles, or as oriented dipoles; indeed, the exact description is still incompletely defined. This phenomenon results in a shift in the electrical potential between the gate and the semiconductor and

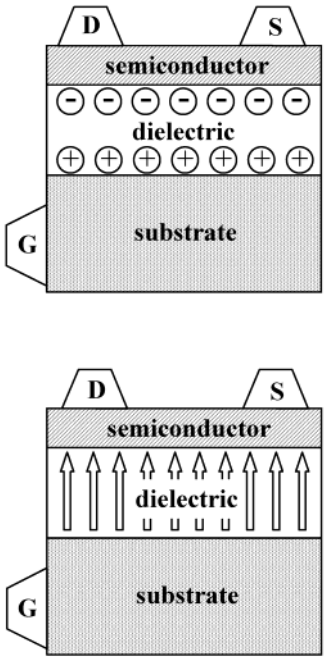

Figure 8. Schematic of an organic transistor, showing the injected static charge after application of a writing voltage as isolated monopoles (top) or as oriented dipoles (bottom).

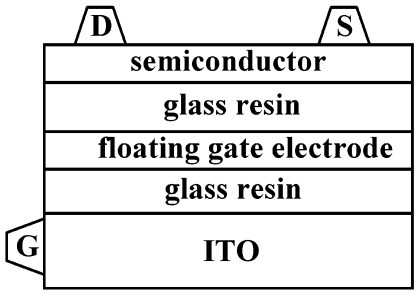

Figure 9. Schematic of a "floating gate" transistor.

alters the charge distribution in the transistor, as illustrated in Figure 8. It appears that the applied depletion voltage, or writing voltage V_w, results in the filling of traps due to the electrostatic attraction of holes to the negatively polarized semiconductor−dielectric interface. This allows for more efficient establishment of the semiconducting channel by majority carriers during operation. Thus, the threshold voltage shifts from accumulation mode (negative for p-type semiconductors, positive for n-type) to zero or even to the depletion mode.

ITO/GR and Si/SiO_2 devices with the same semiconductor behave very differently upon writing; thus, it can be concluded that metal−semiconductor barrier modulations do not play a role. As an example, the effect for dH-PTTP in an Si/SiO_2 device is at least an order of magnitude larger than that in an ITO/GR device. Furthermore, with all Au-semiconductor interfaces identical, the stability of the effect in ITO/GR devices is much greater than that in Si/SiO_2 devices. These observations clearly indicate that the effect involves the dielectric and not the gold-semiconductor interfaces.

To further bound the distribution of the stored charge within the dielectric, ITO/GR devices with a "floating gate" electrode configuration were fabricated.[8] Figure 9 shows a diagram of the floating gate device structure; the only unique feature of such a device (compared to the typical TFT structure) is an additional Au electrode deposited between two separate layers of glass resin. In a standard inorganic memory device with a floating gate structure, this fourth electrode actually stores charge.[8] The purpose of this configuration here, however, is merely to determine whether the stored charge is distributed evenly throughout the dielectric (i.e., identical memory effect observations in floating gate and standard FET devices) or concentrated at the dielectric−semiconductor interface (i.e., greatly reduced or absent memory effect in floating gate devices). The "floating gate" electrode should not affect normal TFT operation. When a writing voltage is applied at the region of the dielectric nearer to the ITO substrate (applied at the gate with respect to a constant voltage at the floating gate), the maximum current increases by only a factor of 3 or less. Such a writing procedure is therefore less effective and less reproducible than the standard procedure using the source and drain electrodes to affect threshold voltage. In addition, current/ratio changes are not monotonic for all gate voltages used to test the device. Nevertheless, these results demonstrate that memory effects must arise primarily from charge stored *near the semiconductor−dielectric interface.*

In a nonvolatile memory element, the required writing voltage depends on the efficiency of the charge storage and the capacitance of the dielectric. In particular, a thinner dielectric would enable writing at a lower voltage, since it is actually the electric *field* across the dielectric that determines the magnitude of charge storage. Also, use of more hydrophobic and/or ferroelectric dielectric composites should increase the stability of charge storage and lower the reversion rate of the transistor. Such materials, including highly fluorinated polymers, are currently under investigation as alternative gate dielectrics for these "nonvolatile" devices. Preliminary results suggest that these polymers do indeed stabilize the adjusted states of the transistors.

Devices were also fabricated using solution-only techniques on ITO substrates, by first applying a spin-coated glass resin and then a solution-cast phenylene−thiophene oligomer and finally painting graphite paste electrodes. Typical channel dimensions for painted electrodes were about 0.5−1 mm (L) and about 5 mm (W). Several devices were fabricated in this way using dH-PTTP (**2**); observed mobilities reached 0.006 $cm^2 V^{-1} s^{-1}$, and on/off ratios for these devices exceeded 10^3. These data are only a factor of 3 lower than those for the analogous devices employing gold electrodes (see Table 3). Only two substrates were prepared from all-solution techniques for compounds **3** and **4**, and the mobilities were within 1 or 2 orders of magnitude of the analogous devices with gold electrodes. One limitation of the graphite electrodes is that they tend to break down more readily, possibly due to delamination from the hydrophobic semiconductor surface. A typical device with painted electrodes could be measured at least several times with no observable deterioration of the electrode contacts, but writing voltages could only be applied 1 or 2 times before the observed current dropped substantially. These preliminary results on ITO/GR using graphite paste are very promising, and alternatives such as polyaniline and PEDOT, which should be less susceptible to delamination, are under investigation.

Conclusions

A new series of mixed phenylene−thiophene oligomers with terminal *n*-hexyl groups has been synthesized and characterized

both as bulk solids and as thin films. The compounds are thermally stable, and the films adopt microstructures with lattice spacings suggestive of molecular alignment along the substrate normal. Morphologies of the vacuum-evaporated films are featureless; however, the morphologies of solution-cast films vary considerably, with highly interconnected crystallites of various shapes and sizes. Both vacuum-evaporated (on Si/SiO_2) and solution-cast (on ITO/GR) films of the compounds exhibit high p-type mobilities, including the straightforwardly prepared compounds **1** and **2**. For compounds **2** and **6**, a significant nonvolatile adjustment of the device characteristics is possible. This memory effect is reversible and tunable by selecting the appropriate writing voltages and writing times. For the first time, evidence demonstrating that most of the effect arises from charge stored near the semiconductor−dielectric interface is deduced from floating gate device experiments. The first all-solution-processed simple nonvolatile elements have been fabricated on ITO substrates, with spin-coated glass resin, solution-cast semiconductors, and conducting graphite paste components; initial results are quite promising.

Acknowledgment. We thank ONR (N00014-02-1-0909) and the NSF-MRSEC program through the Northwestern Materials Research Center (DMR-0076097) for support of this research.

JA035143A